THE JOURNAL OF PHYSICAL CHEMISTRY C

Article

pubs.acs.org/JPCC

Surface Charge of a Nanoparticle Interacting with a Flat Substrate

Selcuk Atalay,[†] Murat Barisik,[‡] Ali Beskok,[‡] and Shizhi Qian[†,*]

[†]Institute of Micro and Nanotechnology, Old Dominion University, Norfolk, Virginia 23529, United States

[‡]Department of Mechanical Engineering, Southern Methodist University, Dallas, Texas 75275, United States

ABSTRACT: Electrostatic interactions between two charged dielectric objects highly depend on their surface charge. Most existing studies assume constant surface charge densities between the two interacting objects regardless of the separation distance between them. The surface charge of a spherical silica nanoparticle interacting with a flat silica plate is investigated numerically as a function of the separation distance normalized with the electrical double layer thickness (κh), pH, and background salt concentration. The numerical model employs Poisson–Nernst–Planck equations for ionic mass transport and considers surface charge regulation in the presence of multiple ionic species. Relatively weak interactions between the nanoparticle and the plate are observed for $\kappa h \gg 1$, resulting in uniform surface charge densities. Because of curvature, the surface charge density of the nanoparticle is higher than that of the plate. Strong interactions are observed for $\kappa h \leq 1$, leading to spatially nonuniform surface charge densities on the nanoparticle and the plate. This effect increases with decreased separation distance (κh). Enhanced proton concentration in the gap between the particle and the plate leads to reduced surface charge densities on the two objects.

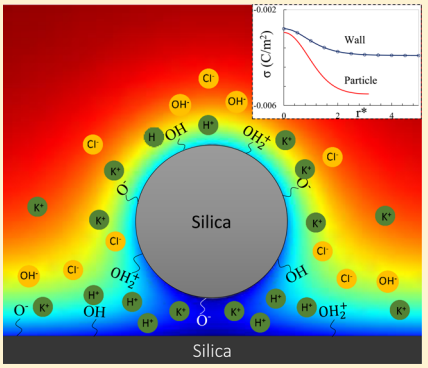

1. INTRODUCTION

Surface charge property of an object in contact with an aqueous solution plays a very important role in the applications of surface science, colloidal science, and electrokinetic transport. For example, electrokinetic transport of ions, fluid, and particles within nanofluidic devices highly depend on the surface charge densities of the channel wall and the nanoparticles.[1−3] Many (bio)particles such as DNA,[4−8] proteins,[9−12] biological molecules,[13,14] and synthetic particles are separated on the basis of their charge differences. Dispersion stability of colloids depends on the charge properties of the colloids, and typically, highly charged colloids are more stable. Cellular uptake of nanoparticles is also affected by the nanoparticle's size and charge. Electrostatic interactions between two objects immersed in an aqueous solution also highly depend on their charge properties.

Surface charge forms as a result of dissociation of ionizable groups or adsorption/reaction of ions at the interface, when an object is in contact with an electrolyte solution.[15] Because the surface reactions including adsorption of ions and protonation/deprotonation depends on the local ionic environment (e.g., local pH and salt concentrations) at the interface, typically the surface charge of an object is not a material property and depends on the local solution properties such as pH, ionic species, and their local concentrations.[16−18] When two charged objects are close to each other, the electrical double layers (EDLs) of the two interacting objects will overlap. Therefore, the local solution properties such as ionic concentrations in the gap between the two interacting objects are different from those when the two objects are sufficiently away from each other. For example, when two negatively charged objects are very close, their EDLs with dominant cations overlap, resulting in enriched cations such as H^+ ions in the interaction region between them. This generates a spatially nonuniform ionic concentration of cations around the interacting objects, yielding nonuniform surface charge properties of the two interacting objects. However, many existing studies assumed that the surface charge properties of two interacting objects remain at their bulk values. For example, the surface charge properties of two interacting objects are assumed to be constants in the well-known Derjaguin–Landau–Verwey–Overbeek (DLVO) theory,[19−23] which has been widely used to fit the measured interaction forces versus separation distances and to estimate the charge properties of two interacting objects.[24−48] Nanoparticles translocating through charged nanopores are commonly observed in nanopore biosensing applications. Most such investigations assume constant surface charges on the nanoparticle and the nanopore.[49,50] Because the EDLs are significantly overlapped in the nanopore, local ionic concentration around the bioparticle and the nanopore can be dramatically different from the conditions when the bioparticle is absent.

The objective of this study is to investigate the variation of the surface charge properties of two interacting silica objects as a function of their normalized separation distance (κh) under various pH and salt concentration. Because the silica nanoparticles have been widely used in colloidal science, biomolecular transport, and drug delivery[44,46,51−59] and because many nanofluidic devices (e.g., nanopores and nanochannels) are made of silica,[60−62] we investigate the charge properties of a

Received: March 7, 2014
Revised: April 20, 2014
Published: April 30, 2014

   dx.doi.org/10.1021/jp5023554 | J. Phys. Chem. C 2014, 118, 10927−10935

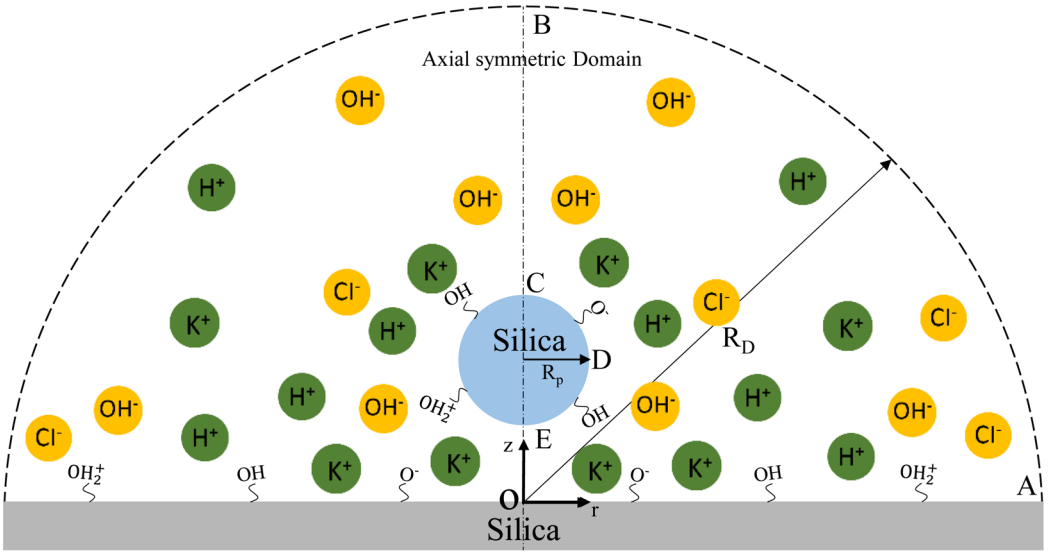

Figure 1. Schematics of a spherical silica nanoparticle interacting with a flat silica plate immersed in an electrolyte solution containing K^+, H^+, Cl^-, and OH^- ionic species.

silica nanoparticle interacting with a silica flat surface. In contrast to most previous studies which neglected the surface chemistry, we analyze the effects of local pH and salt concentrations on the surface charge using a multi-ion charge regulation model.[24,63,64]

2. MATHEMATICAL MODEL

We consider a spherical silica nanoparticle of radius R_p located above a flat silica surface which is immersed inside an electrolyte solution containing N type of ionic species as shown in Figure 1. The separation distance between the bottom pole of the particle and the flat surface is h. We assume that the electrolyte solution includes background salt KCl with a bulk concentration of C_{KCl}, and its acidic and basic solution properties are adjusted by HCl and KOH solutions. Therefore, there are four ionic species, K^+, H^+, Cl^-, and OH^-, in the solution.

Because of the axial symmetry, symmetric cylindrical coordinate system (r, z) with the origin fixed at the center of the flat wall surface is adopted in this study. The electrostatics and ionic mass transport are governed by the steady-state Poisson−Nernst−Planck (PNP) equations:

$$-\varepsilon_0\varepsilon_f\nabla^2\phi = \rho_e = F\sum_{i=1}^{4} z_i c_i \tag{1}$$

and

$$\nabla\cdot\mathbf{N}_i = \nabla\cdot\left(-D_i\nabla c_i - z_i\frac{D_i}{RT}Fc_i\nabla\phi\right) = 0 \quad (i = 1, ..., 4) \tag{2}$$

In the above, ϕ is the electric potential inside the electrolyte solution; c_i, z_i, and D_i are, respectively, the molar concentration, valence, and diffusion coefficient of the ith ionic species (i = 1 for H^+; i = 2 for K^+; i = 3 for Cl^-; and i = 4 for OH^-); F is the Faraday constant; R is the universal gas constant; T is the fluid temperature; ε_0 is the permittivity of the vacuum; ε_f is the relative permittivity of the electrolyte solution; and ρ_e represents the space surface charge density inside the electrolyte solution. Because of the use of the PNP equations, concentration polarization arising from the EDL compression by the nanoparticle and the plate is taken into account in this study.

To solve the coupled eqs 1 and 2, appropriate boundary conditions are required. Along the axis (i.e., r = 0), axial symmetry boundary conditions for electric potential and for each ionic concentration are applied. Far away from the charged nanoparticle and plate (e.g., dashed line AB in Figure 1), we assume that the ionic concentration of each species maintains its bulk concentration, $c_i = C_{i0}$, for i = 1, ..., 4. On the basis of the electroneutrality condition, the bulk concentration for each species is

$$C_{10} = 10^{-pH+3} \quad \text{and} \quad C_{40} = 10^{-(14-pH)+3} \tag{3}$$

$$C_{20} = C_{KCl} \quad \text{and} \quad C_{30} = C_{KCl} + C_{10} - C_{40} \quad \text{when} \quad pH \le 7 \tag{4}$$

and

$$C_{20} = C_{KCl} + C_{10} - C_{40} \quad \text{and} \quad C_{30} = C_{KCl} \quad \text{when} \quad pH > 7. \tag{5}$$

On the rigid surfaces of the nanoparticle and plate, normal ionic flux for each species is zero, $\boldsymbol{n}\cdot\boldsymbol{N}_i = 0$ (i = 1, ..., 4). For the electrical potential, $\phi = 0$ is imposed far away from the charged surfaces. On charged surfaces of nanoparticle and plate, surface charge density boundary condition, $-\varepsilon_0\varepsilon_f\boldsymbol{n}\cdot\nabla\phi = \sigma_w$, is imposed. In contrast to the existing studies using a constant surface charge density regardless of the separation distance between the particle and the plate, in the present work, the surface charge densities of the silica nanoparticle and the plate are determined from the protonation/deprotonation surface reactions of silanol functional groups.[63] Since the characteristic time scale for the protonation/deprotonation process is very short and the relaxation time for electrostatic interaction between ions is about 10^{-13}∼10^{-14} seconds,[65−67] only steady-state ionic mass transport and surface chemical reactions are considered in this study. We assume that the following two protonation reactions of singly Si-coordinated sites with equilibrium constants K_A and K_B occur:

dx.doi.org/10.1021/jp5023554 | J. Phys. Chem. C 2014, 118, 10927−10935

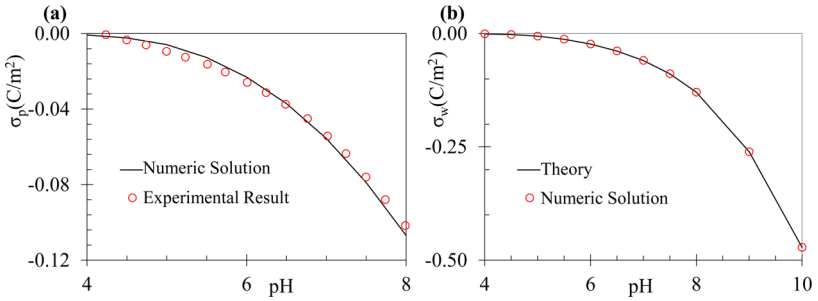

Figure 2. Surface charge densities of (a) silica nanoparticle and (b) a planar silica plate as a function of pH of the electrolyte solution. Circles and line in a represent, respectively, the experimental data from Sonnefeld et al.[69] and the numerical results. Circles and line in b represent, respectively, the numerical results and the analytical results derived by Yeh et al.[63]

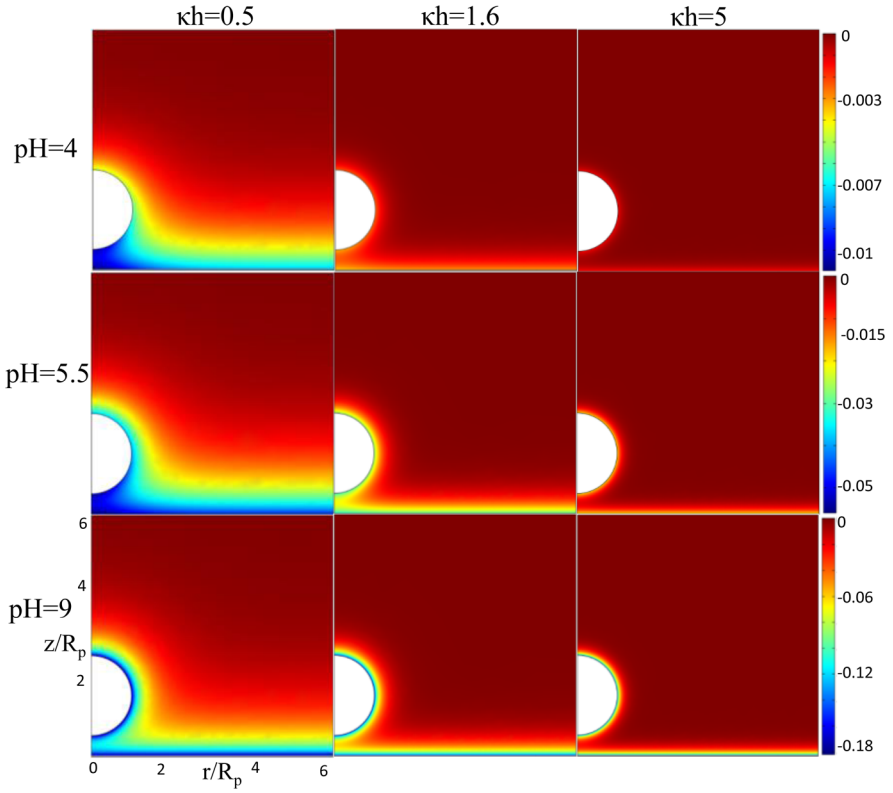

Figure 3. Distribution of the electric potential around the nanoparticle interacting with a flat surface at different κh and pH. Color bars denote the electric potential in volts.

$$\mathrm{SiOH} \leftrightarrow \mathrm{SiO^-} + \mathrm{H^+} \tag{6}$$

and

$$\mathrm{SiOH} + \mathrm{H^+} \leftrightarrow \mathrm{SiOH_2^+} \tag{7}$$

The equilibrium constants are calculated as

$$K_A = \frac{N_{SiO^-}[H^+]_s}{N_{SiOH}} \quad \text{and} \quad K_B = \frac{N_{SiOH_2^+}}{N_{SiOH}[H^+]_s} \tag{8}$$

In the above, N_{SiOH}, N_{SiO^-}, and $N_{SiOH_2^+}$ are the surface site densities of SiOH, SiO^-, and $SiOH_2^+$, respectively. $[H^+]_s$ is the concentration of H^+ ions at the solid/liquid interface. The effects of the Stern layer on determination of surface charge property are neglected in the current work. The total number site density of silanol functional groups on the solid/liquid interface is

$$N_{total} = N_{SiOH} + N_{SiO^-} + N_{SiOH_2^+} \tag{9}$$

On the basis on eqs 8 and 10, the surface charge density on the nanoparticle and the plate can be expressed as

$$\sigma_w = -FN_{total}\frac{K_A - K_B[H^+]_s^2}{K_A + [H^+]_s + K_B[H^+]_s^2} \tag{10}$$

$[H^+]_s$ in eq 10 is the proton concentration on the surface of the particle and plate. Although both are made of the same material with the same N_{total}, K_A, and K_B, their surface charge densities might be different if their local proton concentrations are different. Equation 10 also clearly shows that the surface charge density is not a material property that is due to its dependence on the local proton concentration.

3. NUMERICAL IMPLEMENTATION AND CODE VALIDATION

The PNP equations are numerically solved using a commercial finite-element package COMSOL Multiphysics (www.comsol.

dx.doi.org/10.1021/jp5023554 | J. Phys. Chem. C 2014, 118, 10927−10935

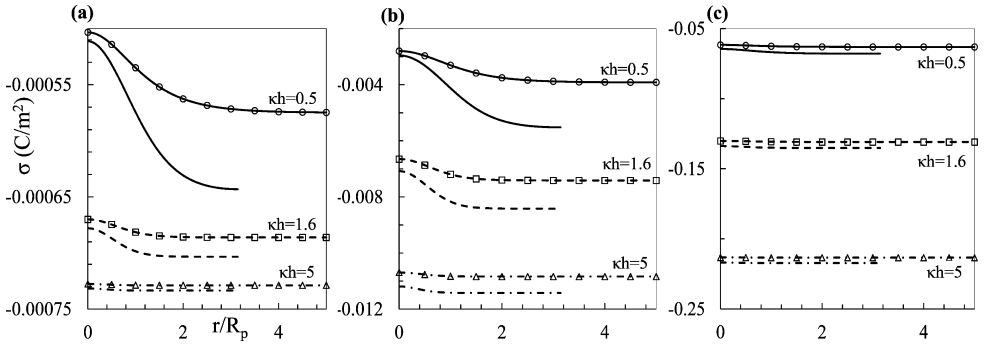

Figure 4. Surface charge densities along the nanoparticle surface (lines without symbols) and the flat plate (lines with symbols) at pH = (a) 4, (b) 5.5, and (c) 9.

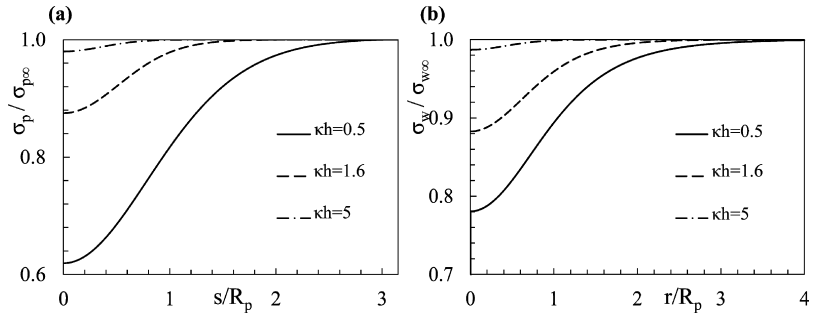

Figure 5. Spatial variation of the normalized surface charge density on (a) nanoparticle and (b) flat plate for different κh values and fixed pH = 5.5.

com) operating in a high-performance cluster. Finer mesh is used around the surfaces of charged nanoparticle and plate and in the gap between the particle and the plate. Relatively coarse mesh is used in regions far away from the charged surfaces. In the simulations, the far field boundary (e.g., dashed line AB in Figure 1) is set as $R_D = 50R_p$, which is sufficiently large, and the results do not change as R_D further increases. Through systematic studies of mesh refinements, mesh independent results are established using about 300 000 Lagrange-quadratic elements in the domain.

Physical parameters used in the simulations are $\varepsilon_0\varepsilon_f = 7.08 \times 10^{-10}$ F/m, $R = 8.31$ J/(K·mol), $F = 96\,490$ C/mol, $T = 300$ K, $N_{total} = 4.816$ sites/nm^2, $pK_A = -\log K_A = 7.0$, and $pK_B = -\log K_B = 1.9$. The diffusivities of H^+, K^+, Cl^-, and OH^- ions are, respectively, 9.31×10^{-9}, 1.96×10^{-9}, 2.03×10^{-9}, and 5.30×10^{-9} m^2/s.[68] The particle radius is $R_p = 10$ nm, and the separation distance between the particle's bottom pole and the flat surface is kept constant for all simulation cases at $h = 5$ nm, and the degree of interaction is adjusted by varying the bulk salt concentration C_{KCl} in the range of 1 −100 mM. The EDL thickness is calculated using $\kappa^{-1} = \lambda_D = (\varepsilon_0\varepsilon_f RT/\sum_{i=1}^{4} F^2 z_i^2 C_{i0})^{1/2}$, and the results are presented as a function of normalized separation distance κh. The pH of the aqueous solution is adjusted by using H^+ or OH^- ionic species in the range of 4−10.

For code validation purposes, we simulated the surface charge density of a spherical silica nanoparticle of $R_p = 58$ nm immersed in an infinite electrolyte medium without the plate. The obtained results illustrated in Figure 2a show good agreement with the experimental data obtained by Sonnefeld et al.[69] for bulk salt concentration $C_{KCl} = 100$ mM, $N_{total} = 2.1$ sites/nm^2, $pK_A = 6.38$, and $pK_B = 1.87$. Therefore, the charge regulation model for the surface charge density captures the underlying physics. We also modeled a flat silica surface in contact with a semi-infinite electrolyte solution. Analytical solution for the surface charge density of a planar surface has been recently derived by Yeh et al.[63] Figure 2b depicts the surface charge density of a planar surface as a function of pH for bulk salt concentration $C_{KCl} = 100$ mM. The numerical results (red circles) are in good agreement with the analytical results (solid line). Clearly, the surface charge density increases with increased pH of the solution.

4. RESULTS AND DISCUSSION

4.1. Salt Concentration Effect. When the interaction between the particle and the plate is very weak, which occurs when the separation distance is much larger than the EDL thickness (i.e., $\kappa h \gg 1$), the surface charge density along the surface of the particle (plate) is spatially uniform. Because of the curvature effect, the surface charge density of the nanoparticle is different from that of the plate. We denote the surface charge densities of the particle and the plate under the condition of no interaction as $\sigma_{p\infty}$ and $\sigma_{w\infty}$, respectively.

The electrostatic interaction between the particle and the plate increases as κh decreases. Figure 3 depicts the electric potential distribution around the nanoparticle and the interacting plate for different pH and κh values. The EDLs are not overlapped for $\kappa h = 5$; therefore, the electric potential along the surface of the particle and the plate is spatially uniform. As κh decreases, the degree of EDL overlap increases. EDLs are slightly overlapped in the gap for $\kappa h = 1.6$, and the magnitude of the electrical potential in the gap region between the particle and the plate is higher than that located far away from the interaction region. EDLs are significantly overlapped for $\kappa h = 0.5$, resulting in a larger interaction region with an enhanced electric potential. Obviously, the electric potential around the particle (plate) becomes significantly nonuniform for $\kappa h \leq 1$ because of serious EDL overlapping. On the particle

dx.doi.org/10.1021/jp5023554 | J. Phys. Chem. C 2014, 118, 10927−10935

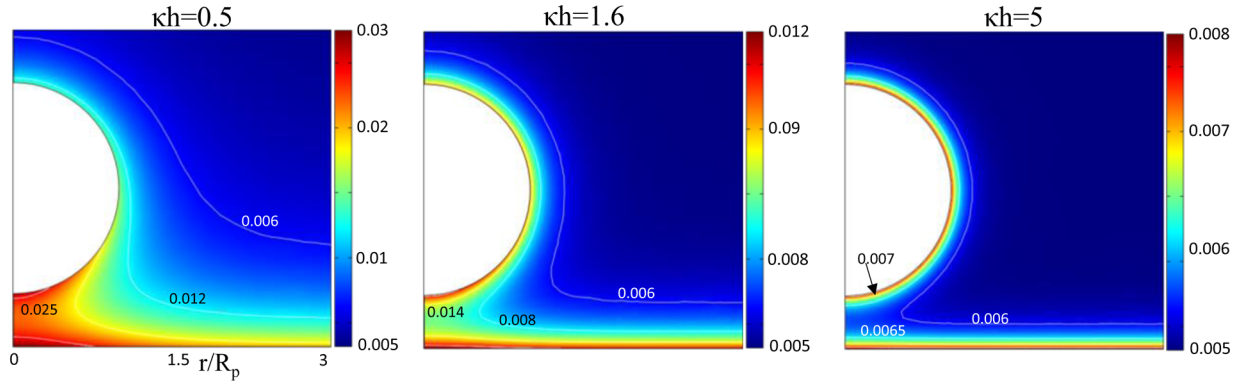

Figure 6. Spatial distribution of H^+ ion concentration (in mM) near the nanoparticle for different κh values and pH = 5.5.

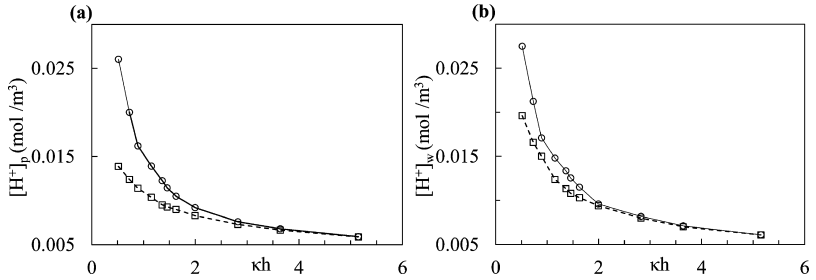

Figure 7. (a) H^+ ion concentration on the particle's top pole (square with dashed line) and on the particle's bottom pole (circle with solid line). (b) H^+ ion concentration on the plate at $r = 0$ (solid line with circles) and $r \rightarrow \infty$ (square with dashed line).

surface, the highest potential occurs at the bottom pole of the particle, where the strongest interaction occurs, and the lowest potential occurs at the top pole which has the weakest interaction with the bottom flat plate. The potential difference between the bottom and top poles of the spherical particle increases as κh decreases for all pH values.

Figure 4 depicts the surface charge densities along the arc length of the particle surface starting from the bottom pole to the top pole (lines without symbols) and along the flat surface (lines with symbols) under the conditions of Figure 3. Under any given condition, the surface charge density of the nanoparticle is typically a little bit higher than that of the plate, and this is attributed to the curvature effect.[64] Under the condition of serious EDL overlap (i.e., $\kappa h = 0.5$), the surface charge densities of the particle and the plate become spatially nonuniform. The magnitude of the surface charge density in the interacting region is typically lower than that far away from the interaction region. As κh increases, the degree of the nonuniform distribution of the surface charge density decreases. In addition, the surface charge densities of the particle and the plate increase with an increase in κh. To further clearly show the variation of the charge density along the particle and the plate, Figure 5 illustrates the spatial distributions of the surface charge densities along the arc length of (a) the particle surface and (b) the plate normalized by the corresponding surface charge densities for $\kappa h \rightarrow \infty$. In the absence of interaction, the normalized surface charge density is 1. Because the top pole of the spherical particle has very weak interaction with the bottom plate under the considered conditions, the normalized surface charge density at the top pole is 1. However, the normalized surface charge density at the bottom pole significantly deviates from 1, especially when the EDLs are significantly overlapped. For example, at $\kappa h = 0.5$, the surface charge density at the bottom pole of the sphere is about 62% of that at the top pole of the nanoparticle. The surface charge density on the plate at $r = 0$ is about 78% of the noninteracting region. Therefore, the assumption of constant surface charge densities of two interacting objects used in previous studies is inappropriate.[50,70] The normalized surface charge density increases on the particle's surface from the bottom toward the top pole. As κh increases, the interaction region decreases; therefore, the region with normalized surface charge density smaller than 1 shrinks. For $\kappa h = 5$, only a small portion of the particle and only a small portion of the plate have very weak interaction, and their normalized surface charge densities are slightly smaller than 1 as shown in Figure 5.

The significant reduction of the surface charge densities of the particle and the plate is attributed to the significant enrichment of positive ions in the interaction region. Under the considered conditions, both the nanoparticle and the plate are negatively charged. Counterions, (K^+ and H^+), are accumulated within each EDL, and co-ions, Cl^- and OH^-, are depleted. Figure 6 depicts the spatial distribution of the concentration of H^+ ions near the nanoparticle for pH = 5.5 at different κh values. The variation of κh is achieved by adjusting the bulk concentration of the background salt, C_{KCl}. Figure 6 shows that the concentration of H^+ ions is significantly enhanced as κh decreases. The enriched positive ions decrease the negatively charged SiO^- dissociated from the functional groups SiOH, yielding lower negative surface charge density in the interaction region.[71,72] Figure 7a depicts ionic concentration of H^+ ions at the bottom (solid line) and top (dashed line) poles of the particle as a function of κh when the pH level is 6.5. Because the increase in κh is achieved by increasing the bulk salt concentration, C_{KCl}, the concentration of K^+ ions also increases with an increase in κh. The increased K^+ ions in the EDL of the nanoparticle repel H^+ ions, resulting in a decrease in the concentration of H^+ inside the EDL. At the top pole of the

dx.doi.org/10.1021/jp5023554 | J. Phys. Chem. C 2014, 118, 10927−10935

nanoparticle, which almost has no interaction with the plate, the concentration of H^+ ions decreases as κh increases, and this is attributed to the depletion of H^+ ions by the increased K^+ ions. When $\kappa h \leq 2$, the concentration of H^+ ions at the bottom pole is much higher than that at the top pole, which is due to the enriched positive ions in the interaction region by EDL overlap. As κh increases, the degree of EDL overlap decreases, and the difference between the proton concentrations at the bottom and top poles decreases. Figure 7b shows the concentration of H^+ ions on the plate at the origin (solid line) and far away from the interaction region (dashed line). Similarly, the proton concentration at the origin where the strongest interaction occurs significantly increases because of the EDLs overlapping. On the basis of the protonation/deprotonation reactions, the surface charge density is inversely proportional to the local concentration of H^+ ions; the enriched H^+ ions in the interaction region arising from the overlapped EDLs lead to lower surface charge density in the interaction region as shown in Figures 4 and 5.

Figure 8 shows the ratio of the surface charge density difference at the top and bottom poles to the surface charge density at the top pole, $(\sigma_{pT} - \sigma_{pb})/\sigma_{pT}$, as a function of κh at pH = 4, 5.5, and 9. At each pH, the surface charge density difference at the top and bottom poles of the particle decreases as κh increases. As κh exceeds a certain critical value, the surface charge density difference vanishes, and the surface charge density is uniformly distributed along the particle surface. At the same κh, the relative surface charge difference at pH = 5.5 is higher than that at pH = 4 and 9, which will be explained in the following section.

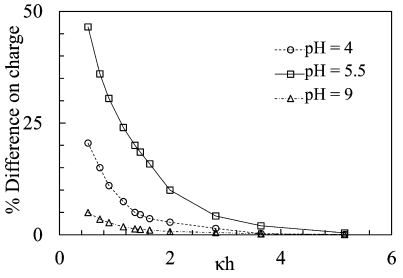

Figure 8. Ratio of the surface charge density difference at the top and bottom poles of the particle to the surface charge density at the top pole as a function of κh for different pH values.

4.2. pH Effect. Previous results clearly show that the surface charge properties of two interacting objects vary with the degree of their interaction, and the surface charge density in the interaction region is dramatically reduced when the EDLs are significantly overlapped. In this section, the effect of pH on the surface charge density of the particle interacting with the plate is investigated at fixed κh = 0.5, 1.6, and 5 where the corresponding bulk salt concentrations are 1, 10, and 100 mM, respectively.

Figure 9a depicts the surface charge density at the bottom pole of the particle as a function of pH at κh = 0.5, 1.6, and 5. At fixed κh, the negative surface charge density increases with an increase in pH. This is expected since the bulk concentration of H^+ ions decreases as pH increases, leading to more SiO^- functional groups dissociated from SiOH. Figure 9b depicts the surface charge density at the bottom pole of the particle normalized by that for $\kappa h \rightarrow \infty$. At κh = 5, the normalized surface charge density is close to 1 because of very weak interaction. However, for κh = 1.6 and 0.5, because of strong interaction, the normalized surface charge density is below 1. The normalized surface charge first decreases as pH increases, attains the minimum at a critical pH, and then increases when pH exceeds the critical value. The variation of the normalized surface charge density with pH can be explained by the variation of the surface concentration of proton under the considered conditions. Figure 10 depicts the concentration of H^+ ions at the bottom pole normalized by that for $\kappa h \rightarrow \infty$ at the same conditions of Figure 9. The normalized surface concentration of H^+ ions increases with an increase in pH when the latter is relatively low, attains a maximum at a critical pH, and then decreases as pH further increases. As pH increases, the bulk concentration of H^+ ions decreases, leading to a decrease in the surface concentration of H^+ ions. However, the negative surface charge density increases as pH increases, which attracts more H^+ ions to the negatively charged surface, resulting in an increase in the surface concentration of H^+ ions.

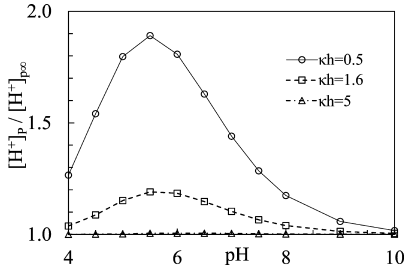

Figure 10. Concentration of H^+ ions at the bottom pole of the particle normalized by that at $\kappa h \rightarrow \infty$ as a function of pH for different κh values.

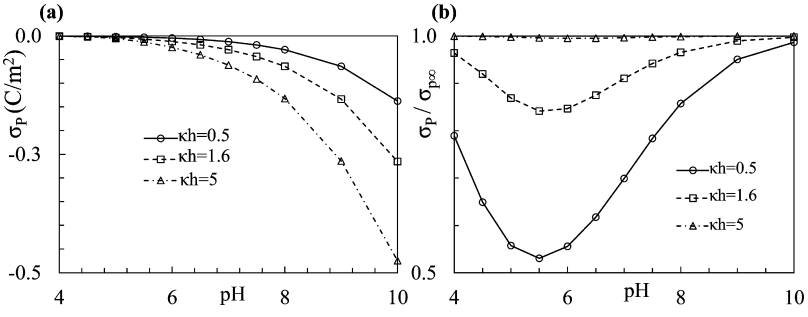

Figure 9. (a) Surface charge density at the bottom pole of the nanoparticle as a function of pH for κh = 0.5, 1.6, and 5. (b) Surface charge density on the bottom pole of the nanoparticle normalized by that at $\kappa h \rightarrow \infty$ as a function of pH for three different κh values.

dx.doi.org/10.1021/jp5023554 | J. Phys. Chem. C 2014, 118, 10927−10935

The variation of the surface concentration of H^+ ions with pH is the net result of the two competitions. When pH is relatively low, because the bulk concentration of H^+ ions is not very low, the increased negative charge attracts a lot of H^+ ions into the overlapped EDLs, resulting in an increase in the concentration of H^+ ions in the interaction region. However, at relatively high pH, the bulk concentration of K^+ ions becomes significantly higher than that of H^+ ions; therefore, more K^+ ions than H^+ ions will be accumulated in the overlapped EDLs. The enriched K^+ ions will also deplete H^+ ions leading to a decrease in H^+ ions inside the EDL. Therefore, the local concentration of H^+ ions at the bottom pole of the particle increases with an increase in pH at relatively low pH, attains the maximum at a critical pH, and then decreases as pH further increases. Because the charge density is inversely proportional to the local concentration of H^+ ions, the surface charge densities of the particle in the interaction region decrease as pH increases and attain the minimum at the critical pH value after which they increase as pH further increases.

5. CONCLUSIONS

Surface charge properties of interacting silica nanoparticle and plate are theoretically investigated as functions of pH, background salt concentration, and the degree of their interaction. The model considers multiple ionic species, charge regulation on the interaction objects, and double layer overlap. The Stern layer effects are not considered in the current study. Without interaction, the surface charge density is homogeneous. However, the charge densities become spatially nonuniform, and the magnitude of the surface charge density in the interaction region is significantly reduced when the double layers are overlapped. Under strong interaction, the surface charge density in the interaction region is only about 50% of the bulk value. Because the degree of interaction increases as the ratio of the separation distance to the EDL thickness, κh, decreases, the deviation from constant charge densities for two interacting objects increases as κh decreases. In the interaction region, the normalized surface charge densities of the particle and the plate decrease as pH increases, attain a minimum value at a critical pH value, and then increase with further increase in pH. This arises from the competition of the following two mechanisms: (1) bulk concentration of H^+ ions decreases as pH increases, yielding to a decrease in the surface concentration of H^+ ions; and (2) the negative surface charge density increases with an increase in pH, which attracts more counterions accumulated inside the EDLs. When more K^+ ions are accumulated than the H^+ ions, the enriched K^+ ions also deplete the H^+ ions. The results demonstrate that the assumption of constant surface charge density of two interacting objects is invalid under strong EDL interactions between the particle and the surfaces in the range of $\kappa h \leq 1$.

AUTHOR INFORMATION

Corresponding Author

*E-mail: sqian@odu.edu. Phone: 757-683-3304. Fax: 757-683-3200.

Notes

The authors declare no competing financial interest.

REFERENCES

(1) Sang, J. M.; Du, H. T.; Wang, W.; Chu, M.; Wang, Y. D.; Li, H. C.; Zhang, H. A.; Wu, W. G.; Li, Z. H. Protein Sensing by Nanofluidic Crystal and its Signal Enhancement. *Biomicrofluidics* **2013**, *7*, 024112.

(2) Cheng, L. J.; Guo, L. J. Ionic Current Rectification, Breakdown, and Switching in Heterogeneous Oxide Nanofluidic Devices. *ACS Nano* **2009**, *3*, 575−584.

(3) Perry, J. M.; Zhou, K. M.; Harms, Z. D.; Jacobson, S. C. Ion Transport in Nanofluidic Funnels. *ACS Nano* **2010**, *4*, 3897−3902.

(4) Jenison, R.; Yang, S.; Haeberli, A.; Polisky, B. Interference-based Detection of Nucleic Acid Targets on Optically Coated Silicon. *Nat. Biotechnol.* **2001**, *19*, 62−65.

(5) Ullien, D.; Cohen, H.; Porath, D. The Effect of the Number of Parallel DNA Molecules on Electric Charge Transport through 'Standing DNA'. *Nanotechnology* **2007**, *18*, 424015.

(6) Baumgartner, S.; Vasicek, M.; Bulyha, A.; Heitzinger, C. Optimization of Nanowire DNA Sensor Sensitivity using Self-Consistent Simulation. *Nanotechnology* **2011**, *22*, 425503.

(7) Chang, H.; Kosari, F.; Andreadakis, G.; Alam, M. A.; Vasmatzis, G.; Bashir, R. DNA-Mediated Fluctuations in Ionic Current through Silicon Oxide Nanopore Channels. *Nano Lett.* **2004**, *4*, 1551−1556.

(8) Pu, Q. S.; Oyesanya, O.; Thompson, B.; Liu, S. T.; Alvarez, J. C. On-chip Micropatterning of Plastic (Cylic Olefin Copolymer, COC) Microfluidic Channels for the Fabrication of Biomolecule Microarrays using Photografting Methods. *Langmuir* **2007**, *23*, 1577−1583.

(9) Duffy, C. F.; Gafoor, S.; Richards, D. P.; Admadzadeh, H.; O'Kennedy, R.; Arriaga, E. A. Determination of properties of Individual Liposomes by Capillary Electrophoresis with Postcolumn Laser-Induced Fluorescence Detection. *Anal. Chem.* **2001**, *73*, 1855−1861.

(10) Miura, A.; Tanaka, R.; Uraoka, Y.; Matsukawa, N.; Yamashita, I.; Fuyuki, T. The Characterization of a Single Discrete Bionanodot for Memory Device Applications. *Nanotechnology* **2009**, *20*, 125702.

(11) Chen, M. Y.; Sailor, M. J. Charge-Gated Transport of Proteins in Nanostructured Optical Films of Mesoporous Silica. *Anal. Chem.* **2011**, *83*, 7186−7193.

(12) Ali, M.; Bayer, V.; Schiedt, B.; Neumann, R.; Ensinger, W. Fabrication and Functionalization of Single Asymmetric Nanochannels for Electrostatic/Hydrophobic Association of Protein Molecules. *Nanotechnology* **2008**, *19*, 485711.

(13) Liang, L.; Rulis, P.; Ching, W. Y. Mechanical Properties, Electronic Structure and Bonding of Alpha- and Beta-tricalcium Phosphates with Surface Characterization. *Acta Biomater.*. **2010**, *6*, 3763−3771.

(14) Lopes, M.; Candini, A.; Urdampilleta, M.; Reserbat-Plantey, A.; Bellini, V.; Klyatskaya, S.; Marty, L.; Ruben, M.; Affronte, M.; Wernsdorfer, W.; et al. Surface-Enhanced Raman Signal for Terbium Single-Molecule Magnets Grafted on Graphene. *ACS Nano* **2010**, *4*, 7531−7537.

(15) Hunter, R. J. *Zeta Potential in Colloid Science: Principles and Applications*; Academic Press: London, 1981; Vol. *125*.

(16) Barr, S. A.; Panagiotopoulos, A. Z. Interactions Between Charged Surfaces with Ionizable Sites. *Langmuir* **2011**, *27*, 8761−8766.

(17) Prieve, D. C.; Ruckenstein, E. The Surface Potential of and Double-Layer Interaction Force Between Surfaces Characterized by Multiple Ionizable Groups. *J. Theor. Biol.* **1976**, *56*, 205−228.

(18) Baldessari, F. Electrokinetics in Nanochannels - Part II. Mobility dependence on Ion Density and Ionic Current Measurements. *J. Colloid Interface Sci.* **2008**, *325*, 539−546.

(19) Verwey, E. J. W. Theory of the Stability of Lyophobic Colloids. *J. Colloid Interface Sci.* **1947**, *51*, 631−636.

(20) Derjaguin, B.; Landau, L. The Theory of Stability of Highly Charged Lyophobic Sols and Coalescence of Highly Charged Particles in electrolyte solutions. *Zh. Eksp. Teor. Fiz.* **1941**, *11*, 802−821.

(21) Verwey, E. J. W.; Overbeek, J. T. G.; Van Nes, K. *Theory of the Stability of Lyophobic Colloids: The Interaction of Sol Particles Having an Electric Double Layer*; Elsevier: New York, 1948.

(22) Israelachvili, J. N. *Intermolecular and Surface Forces: Revised*, 3rd ed.; Academic Press: Waltham, MA, 2011.

(23) Ōhshima, H.; Furusawa, K. *Electrical Phenomena and Interfaces: Fundamentals, Measurements, and Applications*; CRC Press: Hoboken, New Jersey, 1998.

(24) Yeh, L.-H.; Zhang, M.; Hu, N.; Joo, S. W.; Qian, S.; Hsu, J.-P. Electrokinetic Ion and Fluid Transport in Nanopores Functionalized by Polyelectrolyte Brushes. *Nanoscale* **2012**, *4*, 5169−5177.
(25) Bowen, W. R.; Doneva, T. A.; Stoton, J. A. G. The Use of Atomic Force Microscopy to Quantify Membrane Surface Electrical Properties. *Colloids Surf., A: Physicochem. Eng. Aspects* **2002**, *201*, 73−83.
(26) Chen, L.; Conlisk, A. T. DNA Nanowire Translocation Phenomena in Nanopores. *Biomed. Microdevices* **2010**, *12*, 235−245.
(27) Das, S.; Dubsky, P.; van den Berg, A.; Eijkel, J. C. Concentration Polarization in Translocation of DNA through Nanopores and Nanochannels. *Phys. Rev. Lett.* **2012**, *108*, 138101.
(28) Drelich, J.; Long, J.; Yeung, A. Determining Surface Potential of the Bitumen-Water Interface at Nanoscale Resolution Using Atomic Force Microscopy. *Can. J. Chem. Eng.* **2007**, *85*, 625−634.
(29) Duan, J. M. Interfacial Forces between Silica Surfaces Measured by Atomic Force Microscopy. *J. Environ. Sci.* **2009**, *21*, 30−34.
(30) Wang, Y. H.; Wang, L. G.; Hampton, M. A.; Nguyen, A. V. Atomic Force Microscopy Study of Forces between a Silica Sphere and an Oxidized Silicon Wafer in Aqueous Solutions of NaCl, KCl, and CsCl at Concentrations up to Saturation. *J. Phys. Chem. C* **2013**, *117*, 2113−2120.
(31) Lima, E. R.; Bostrom, M.; Schwierz, N.; Sernelius, B. E.; Tavares, F. W. Attractive Double-Layer Forces between Neutral Hydrophobic and Neutral Hydrophilic Surfaces. *Phys. Rev. E: Stat., Nonlinear, Soft Matter Phys.* **2011**, *84*, 061903.
(32) Xu, Z. H.; Chi, R.; Difeo, T.; Finch, J. A. Surface Forces between Sphalerite and Silica Particles in Aqueous Solutions. *J. Adhes. Sci. Technol.* **2000**, *14*, 1813−1827.
(33) Ruiz-Cabello, F. J. M.; Maroni, P.; Borkovec, M. Direct Measurements of Forces between Different Charged Colloidal Particles and their Prediction by the Theory of Derjaguin, Landau, Verwey, and Overbeek (DLVO). *J. Chem. Phys.* **2013**, *138*, 234705.
(34) Larson, I.; Drummond, C. J.; Chan, D. Y. C.; Grieser, F. Direct Force Measurements between Dissimilar Metal-Oxides. *J. Phys. Chem.* **1995**, *99*, 2114−2118.
(35) Miklavic, S.; Chan, D. Y.; White, L.; Healy, T. W. Double Layer Forces Between Heterogeneous Charged Surfaces. *J. Phys. Chem.* **1994**, *98*, 9022−9032.
(36) Popa, I.; Sinha, P.; Finessi, M.; Maroni, P.; Papastavrou, G.; Borkovec, M. Importance of Charge Regulation in Attractive Double-Layer Forces between Dissimilar Surfaces. *Phys. Rev. Lett.* **2010**, *104*, 228301.
(37) Butt, H.-J.; Cappella, B.; Kappl, M. Force Measurements with the Atomic Force Microscope: Technique, Interpretation and Applications. *Surf. Sci. Rep.* **2005**, *59*, 1−152.
(38) Notley, S. M.; Norgren, M. Measurement of Interaction Forces between Lignin and Cellulose as a Function of Aqueous Electrolyte Solution Conditions. *Langmuir* **2006**, *22*, 11199−11204.
(39) Montes Ruiz-Cabello, F. J.; Maroni, P.; Borkovec, M. Direct Measurements of Forces Between Different Charged Colloidal Particles and Their Prediction by the Theory of Derjaguin, Landau, Verwey, and Overbeek (DLVO). *J. Chem. Phys.* **2013**, *138*, 234705.
(40) Elmahdy, M. M.; Drechsler, A.; Gutsche, C.; Synytska, A.; Uhlmann, P.; Kremer, F.; Stamm, M. Forces Between Blank Surfaces As Measured by the Colloidal Probe Technique and by Optical Tweezers - A Comparison. *Langmuir* **2009**, *25*, 12894−12898.
(41) Briscoe, W. H.; Horn, R. G. Direct Measurement of Surface Forces due to Charging of Solids Immersed in a Nonpolar Liquid. *Langmuir* **2002**, *18*, 3945−3956.
(42) Velegol, D.; Thwar, P. K. Analytical Model for the Effect of Surface Charge Nonuniformity on Colloidal Interactions. *Langmuir* **2001**, *17*, 7687−7693.
(43) Zhong, S.; Li, H.; Chen, X. Y.; Cao, E. H.; Jin, G.; Hu, K. S. Different Interactions between the Two Sides of Purple Membrane with Atomic Force Microscope tip. *Langmuir* **2007**, *23*, 4486−4493.
(44) Butt, H. J. Measuring Electrostatic, Vanderwaals, and Hydration Forces in Electrolyte-Solutions with an Atomic Force Microscope. *Biophys. J.* **1991**, *60*, 1438−1444.
(45) Butt, H.-J. Measuring Local Surface Charge Densities in Electrolyte Solutions with a Scanning Force Microscope. *Biophys. J.* **1992**, *63*, 578−582.
(46) Huettl, G.; Beyer, D.; Müller, E. Investigation of Electrical Double Layers on SiO_2 Surfaces by Means of Force vs. Distance Measurements. *Surf. Interface Anal.* **1997**, *25*, 543−547.
(47) Zhou, K.; Perry, J. M.; Jacobson, S. C. Transport and Sensing in Nanofluidic Devices. *Annu. Rev. Anal. Chem.* **2011**, *4*, 321−341.
(48) Pelto, J. M.; Haimi, S. P.; Siljander, A. S.; Miettinen, S. S.; Tappura, K.; Higgins, M. J.; Wallace, G. G. Surface Properties and Interaction Forces of Biopolymer Doped Conductive Polypyrrole Surfaces by Atomic Force Microscopy. *Langmuir* **2013**, *29*, 6099−6108.
(49) Zhang, M.; Yeh, L.-H.; Qian, S.; Hsu, J.-P.; Joo, S. W. DNA Electrokinetic Translocation through a Nanopore: Local Permittivity Environment Effect. *J. Phys. Chem. C* **2012**, *116*, 4793−4801.
(50) Ai, Y.; Qian, S. Electrokinetic Particle Translocation through a Nanopore. *Phys. Chem. Chem. Phys.* **2011**, *13*, 4060−4071.
(51) Ducker, W. A.; Senden, T. J.; Pashley, R. M. Direct Measurement of Colloidal Forces using an Atomic Force Microscope. *Nature* **1991**, *353*, 239−241.
(52) Zhmud, B.; Meurk, A.; Bergström, L. Evaluation of Surface Ionization Parameters from AFM Data. *J. Colloid Interface Sci.* **1998**, *207*, 332−343.
(53) Rutland, M. W.; Senden, T. J. Adsorption of the Poly (oxyethylene) Nonionic Surfactant C12E5 to Silica: a Study Using Atomic Force Microscopy. *Langmuir* **1993**, *9*, 412−418.
(54) Hoh, J. H.; Revel, J.-P.; Hansma, P. K. Tip-Sample Interactions in Atomic Force Microscopy: I. Modulating Adhesion Between Silicon Nitride and Glass. *Nanotechnology* **1991**, *2*, 119.
(55) Ducker, W. A.; Senden, T. J.; Pashley, R. M. Measurement of Forces in Liquids using a Force Microscope. *Langmuir* **1992**, *8*, 1831−1836.
(56) Weisenhorn, A.; Maivald, P.; Butt, H.-J.; Hansma, P. Measuring Adhesion, Attraction, and Repulsion Between Surfaces in Liquids with an Atomic-Force Microscope. *Phys. Rev. B* **1992**, *45*, 11226.
(57) Lin, X. Y.; Creuzet, F.; Arribart, H. Atomic Force Microscopy for Local Characterization of Surface Acid-Base Properties. *J. Phys. Chem.* **1993**, *97*, 7272−7276.
(58) Meagher, L. Direct Measurement of Forces Between Silica surfaces in Aqueous $CaCl_2$ Solutions using an Atomic Force Microscope. *J. Colloid Interface Sci.* **1992**, *152*, 293−295.
(59) Toikka, G.; Hayes, R. A.; Ralston, J. Adhesion of Iron Oxide to Silica Studied by Atomic Force Microscopy. *J. Colloid Interface Sci.* **1996**, *180*, 329−338.
(60) Guégan, R.; Morineau, D.; Alba-Simionesco, C. Interfacial structure of an H-bonding Liquid Confined into Silica Nanopore with Surface Silanols. *Chem. Phys.* **2005**, *317*, 236−244.
(61) Yeh, L. H.; Zhang, M. K.; Qian, S. Z. Ion Transport in a pH-Regulated Nanopore. *Anal. Chem.* **2013**, *85*, 7527−7534.
(62) Yasui, T.; Rahong, S.; Motoyama, K.; Yanagida, T.; Wu, Q.; Kaji, N.; Kanai, M.; Doi, K.; Nagashima, K.; Tokeshi, M.; et al. DNA Manipulation and Separation in Sublithographic-Scale Nanowire Array. *ACS Nano* **2013**, *7*, 3029−3035.
(63) Yeh, L.-H.; Xue, S.; Joo, S. W.; Qian, S.; Hsu, J.-P. Field Effect Control of Surface Charge Property and Electroosmotic Flow in Nanofluidics. *J. Phys. Chem. C* **2012**, *116*, 4209−4216.
(64) Barisik, M.; Atalay, S.; Beskok, A.; Qian, S. Size Dependent Surface Charge Properties of Silica Nanoparticles. *J. Phys.Chem. C* **2014**, *118*, 1836−1842.
(65) Qiao, W. C.; Yang, K. J.; Thoma, A.; Dekorsy, T. Dielectric Relaxation of HCl and NaCl Solutions Investigated by Terahertz Time-Domain Spectroscopy. *J. Infrared, Millimeter, Terahertz Waves* **2012**, *33*, 1029−1038.
(66) Renou, R.; Ding, M.; Zhu, H.; Szymczyk, A.; Malfreyt, P.; Ghoufi, A. Concentration Dependence of the Dielectric Permittivity, Structure and Dynamics of Aqueous NaCl Solutions: Comparison Between the Drude Oscillator and Electronic Continuum Models. *J. Phys. Chem. B* **2014**, *118*, 3931−3940.

(67) Taskiran, A.; Schirmeisen, A.; Fuchs, H.; Bracht, H.; Roling, B. Time-domain Electrostatic Force Spectroscopy on Nanostructured Lithium-ion Conducting Glass Ceramics: Analysis and Interpretation of Relaxation Times. *Phys. Chem. Chem. Phys.* **2009**, *11*, 5499−5505.
(68) Andersen, M. B.; Frey, J.; Pennathur, S.; Bruus, H. Surface-dependent Chemical Equilibrium Constants and Capacitances for Bare and 3-cyanopropyldimethylchlorosilane Coated Silica Nanochannels. *J. Colloid Interface Sci.* **2011**, *353*, 301−310.
(69) Sonnefeld, J.; Löbbus, M.; Vogelsberger, W. Determination of Electric Double Layer Parameters for Spherical Silica particles Under Application of the Triple Layer Model using Surface Charge Density Data and Results of Electrokinetic Sonic Amplitude Measurements. *Colloids Surf., A* **2001**, *195*, 215−225.
(70) Zhang, M.; Ai, Y.; Sharma, A.; Joo, S. W.; Kim, D. S.; Qian, S. Electrokinetic Particle Translocation Through a Nanopore Containing a Floating Electrode. *Electrophoresis* **2011**, *32* (14), 1864−1874.
(71) Jiménez-Ángeles, F. Effects of Mixed Discrete Surface Charges on the Electrical Double Layer. *Phys. Rev. E* **2012**, *86*, 021601.
(72) Atalay, S.; Ma, Y.; Qian, S. Analytical Model for Charge Properties of Silica Particles. *J. Colloid Interface Sci.* **2014**, *425*, 128−130.